

Analytical and Numerical Models for the Aerodynamic Noise Prediction of an High-Speed Train Pantograph

M. VISCARDI, D. SIANO, P. NAPOLITANO

Abstract— The present work deals with the aeroacoustic analysis of a three-dimensional pantograph model, through the employment of an innovative analytical approach and a 3D numerical modeling.

Specifically, the proposed analytical approach, aimed to predict the noise emission, is based on a modified formulation of the Smith and Chow's formula. Namely, by considering the entire landing gear structure as a sum of cylindrical elements, each cylinder noise has been individually calculated by the formula, as a result, based on the superposition principle, the whole noise is obtained; considering that the pantograph can also be considered as a sum of cylindrical elements, this formula, initially developed for aircraft landing gears, has been optimized and calibrated for the purpose of the present study.

Because of, the analytical formula does not take obviously into account several effects related to the noise generation mechanism, a 3D numerical aeroacoustic model of the pantograph was needed. Specifically, the theoretical background adopted is the Williams and Hawkings acoustic analogy, an evolution of the well-known Lighthill acoustic analogy. The latter consists in the substitution of the noise generating surface with a distribution of dipole punctual sound sources, whose intensity is proportional to the temporal variation of fluid dynamic quantities acting in that point. As a result, a more detailed characterization of the noise spectrum can be provided.

The analytical and numerical results have been then compared in terms of sound pressure levels and a well spectral contents, to themselves and to available experimental data.

Keywords—Aerodynamic noise, Radiated Noise, 3D CFD analysis, Aeroacoustic, Pantograph.

I. INTRODUCTION

TWENTY years of study on train noise proves that railway pass-by noise is primarily dominated by three types of noise sources:

- vehicle traction and auxiliary systems
- rolling noise
- aerodynamic noise

Although impact noise and curve squeal can be relevant, they are localized track-related sources, and so of no interest to the determination of the pass-by noise levels on smooth and straight track.

Generally, each of the three mentioned main noise sources have a different speed dependency, related to the kind of

M. Viscardi is Assistant Professor at University of Naples "Federico II", Naples, Italy, (phone: +39-081-7683572; fax: +39-081-624609; e-mail: massimo.viscardi@unina.it). D. Siano is a researcher of Istituto Motori CNR (National research Council) of Italy (e-mail: d.siano@im.cnr.it).

rolling stock concerned.

- At speeds below 60km/h, often traction and auxiliary system noise dominate, if present. It normally has only zero or slight speed dependency of $0-20\log_{10}V$.
- In the medium speed range 60-200km/h, wheel-rail rolling noise will usually dominate, its level depending on the wheel and track roughness level. The speed dependency can vary between $20-30\log_{10}V$.
- At speeds of 200km/h and above, aerodynamic noise becomes more predominant, with a speed dependency of between $50-70\log_{10}V$.

As they are general trends, some exceptions can be found. Firstly, each of these sources has one or more source heights, for example traction noise of a diesel electric locomotive may originate from the vents on the side of the vehicle and from the exhaust at the top. Rolling noise is radiated primarily by the wheels and the track (rails and sleepers), and is therefore located at rail height and axle height. Aerodynamic noise can originate from various heights such as the undercarriage, gaps between carriages, the front and rear of the vehicle, the pantographs and their assembly. An example of the general trends of the various sources is shown in Figure 1.

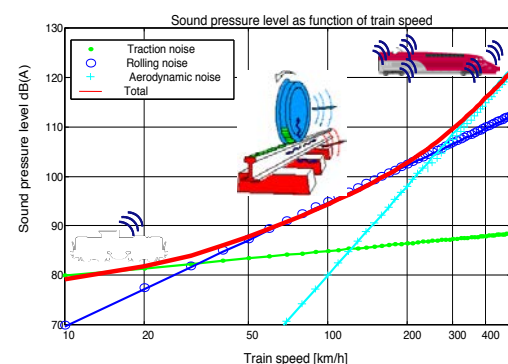


Fig. 1 Speed dependence of different kind of noises

Rolling noise is the main noise source at low train speed: it is due to the contact (and its relative friction) between the wheel and the rail and it changes with V . Traction noise it is substantially an engine noise and it usually do not overcome a sound pressure level of 90dB.

If the vehicle(s) under test satisfies one of these two requisites:

- have a maximum speed of more than 200km/h
- produce aerodynamic noise noticeably higher than the combined rolling noise and traction noise at high speeds,
- the aerodynamic noise is measured.

The second point can be checked as follows: if the measured sound pressure (of all sources) at high speeds (above 200km/h) exceeds the combined traction and rolling noise by more than 1dB, aerodynamic noise is to be measured.

Aerodynamic noise is measured at two or more speeds at which it is known that it is dominant, and preferably with a difference of at least 50km/h, for example 250km/h and 300km/h.

The development of high speed train put the aerodynamic noise in a central position in the studies on train noise optimization; recent papers (Yang & Yang, 2012) show that the aerodynamic noise is becoming more and more the primary noise source, due to the increase in train speed; in particular the aerodynamic noise grows with V^6 where V is the train speed; at high speed ($V > 250$ [km/h]), it is the main noise source.

The aerodynamic noise is the most difficult to model and its experimental characterization requires special test set up and instrumentation.

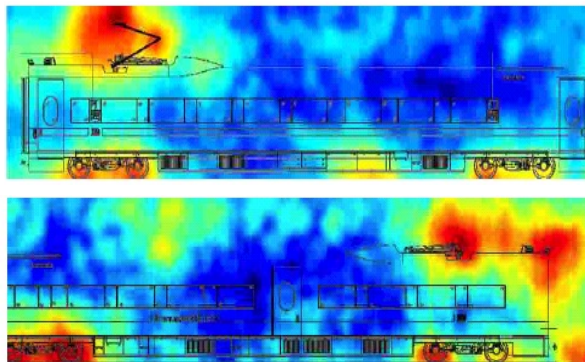


Fig. 2 – Example of an acoustic pressure distribution at 330km/h

In the Figure 1 are shown the main aerodynamic noise source of an high speed train (Yang & Yang, 2012), we can detect three distinct zones: the bogies zone (in this case its aerodynamic noise is overlapped by the rolling noise), the zones where there are the links between carriages, the front of the train (when it is not well aerodynamically designed), the pantograph.

In figure 3 is shown a typical beam forming result on a high speed train's pantograph in wind tunnel.

According to recent studies, the pantograph is probably the principal aerodynamic noise source in high speed trains: this is due to the fact that it is a squat object placed on the top of the train invested by a high speed flow, in this condition 3D vortex shedding phenomena occur and the noise generated

from the relative turbulence is high.

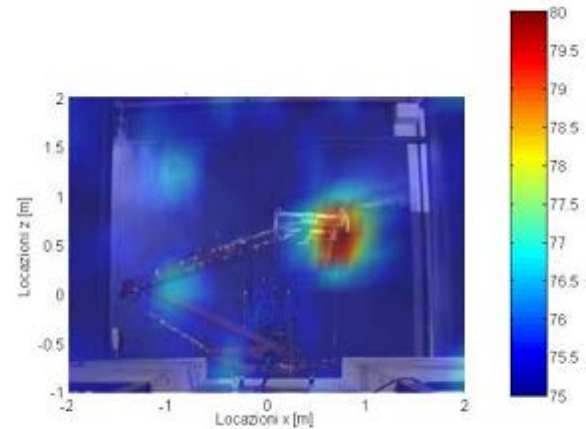


Figure 1 – Measured noise for a high speed train in wind tunnel with beam forming approach

For this reason, train manufacturers created some regulations about noise generated by the pantograph in terms of sound pressure level or sound power level at different train speed; this documents states that the A-weighted sound power level (dB re. $1e-12$ W) from the raised as well as from the lowered pantograph at any position of the train of a train set when the train is running at the given speeds shall not exceed well defined limits (for example for new high speed train):

- 300km/h $L_{wA} = 114$ dB(A)
- 320km/h $L_{wA} = 116$ dB(A)
- 360km/h $L_{wA} = 119$ dB(A)

The A-weighted sound power level (dB re. $1e-12$ W) in 1/3-octave bands from 31.5 Hz to 8 kHz shall be determined with wind tunnel measurements or with a validated numerical aeroacoustic prediction tool.

Test/calculation results from similar pantograph designs can only be used, if the design differences and their anticipated effect on noise generation are clearly stated and the acoustic expert from Bombardier accepts the basis and documentation of differences and effects on noise generation.

II. REFERENCES TO AEROACOUSTIC

Mallock was the first one to explain how wind noise derives from alternatively detaching vortexes in an object wake submerged in a fluid flow (Mallock, 1911).

Considering a circular cylinder invested by a uniform velocity V_∞ (the cylinder diameter is d); if Reynolds number, considering d as the characteristic parameter, is less than 40, then the experience shows that the flow past the cylinder is stationary, while for $Re > 40$ the flow is non stationary due to instabilities.

The non stationary fluid flow configuration is characterized by a double counter-rotating vortex that alternatively detaches

from the body and is transported downriver by the flow. For $50 < Re < 150$ this structure is well organized and it is called Von Karman wake. Basing on acoustic experimentation, Strouhal discovered the relation between vortex shedding frequency f_s , the asymptotic speed V_∞ and the cylinder diameter d_s

$$S_t = \frac{f d_s}{v} \quad (1)$$

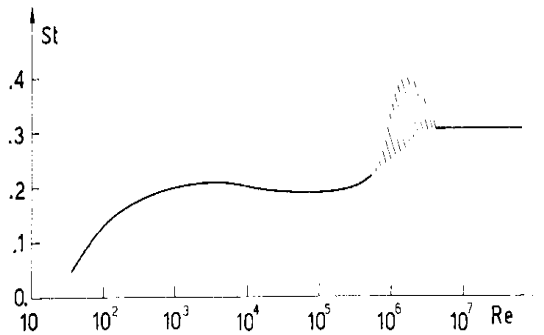


Fig. 4 – ST-RE relation for a cylinder

the S_t parameter is called Strouhal Number. As shown in figure 4, this result, obtained for Reynolds Number between 50 and 150, can be extended also outside this interval.

One of the first consequences of this discovery was the explanation of the Aeolian Harps, as the ancient Greeks called the pure sound emitted by harp strings exposed to a particular wind flow.

An object in a flow induces drag and lift forces parallel and normal to the flow. The alternative detachment of the vortex generates an asymmetry in the flow with a certain periodicity. The obstacle plays the role of a dipole acoustic source.

III. PANTOGRAPH'S DEFINITION AND STRUCTURE

In order to study the aerodynamic noise of the pantograph, it is important to know the structure of the pantograph and how does it works.

A pantograph for rail lines is a hinged electric-rod device that collects electric current from overhead lines for electric trains or trams. The pantograph typically connects to a one-wire line, with the track acting as the ground wire. The term stems from the resemblance to pantograph lever-rod devices for copying handwriting and drawings.

The most common type of pantograph today is the so called half-pantograph (sometimes 'Z'-shaped, see), which has evolved to provide a more compact and responsive single-arm design at high speeds as trains get faster. The half-pantograph can be seen in use on everything from very fast trains (such as the TGV) to low-speed urban tram systems. The design operates with equal efficiency in either direction of motion.



Fig. 5 – Typical "half-pantograph" configuration

The pantograph has thousands of components, but its main elements can be schematized as cylinders.

Generally speaking, if referring to aeroacoustic noise sources, the pantograph can be divided into 3 main components (most of the pantographs can be schematized this way):

- The Arm

It is the lowest component of the pantograph, it is connected to the upper surface of the train and its movement determines the operating height of the pantograph. Usually it is moved through the use of linear actuators such as pistons.

The pantograph's arm for the reference pantograph, is shown in Figure 6.



Fig. 6 – Pantograph's Arm

- The Trapezium

The trapezium is the element that connects the arc with the arm. It is structured by two long cylinders in the flow direction linked together with transversal cylinders and a couple of tie rods.

The pantograph's trapezium is shown in Figure 7 .

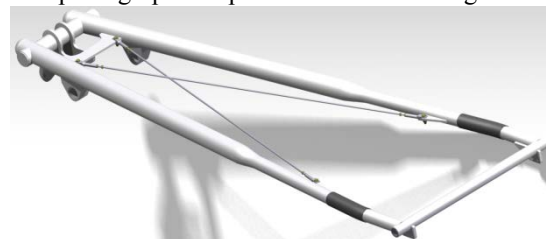


Fig. 7 – Pantograph's Trapezium

- The Arc

It is the core of the entire system: it is put on the top of the pantograph and its main components are two arcs placed perpendicularly to the train length; these arcs touch the wires and are responsible for the electricity link.

The pantograph's arc is shown in Figure 8 .

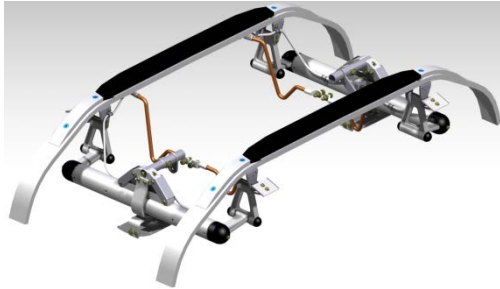


Fig. 8 – V300 Zefiro pantograph's Arc

IV. HOW A PANTOGRAPH WORKS

The electric transmission system for modern electric rail systems consists of an upper weight carrying wire (known as catenary) from which is suspended a contact wire. The pantograph is spring-loaded and pushes a contact shoe against the contact wire to draw the electricity needed to run the train. The steel rails on the tracks act as the electrical return.

Pantographs are the successor technology to trolley poles, which were widely used on early streetcar systems. Trolley poles are still used by trolleybuses, whose freedom of movement and need for a two-wire circuit makes pantographs impractical, and some streetcar networks, such as the Toronto Streetcar System, which have frequent turns sharp enough to require additional freedom of movement in their current collection to ensure unbroken contact. Pantographs with overhead wires are now the dominant form of current collection for modern electric trains because, although more expensive and fragile than a third-rail system, they allow the use of higher voltages.

Pantographs are typically operated by compressed air from the vehicle's braking system, either to raise the unit and hold it against the conductor or, when springs are used to affect the extension, to lower it. As a precaution against loss of pressure in the second case, the arm is held in the down position by a catch. For high-voltage systems, the same air supply is used to "blow out" the electric arc when roof-mounted circuit breakers are used.

V. REFERENCE EXPERIMENTAL DATA

The reference data used inside this activity, derived from a previous detailed study included in an European project contest.

Experimental acoustic measurements have been performed on the pantograph model SSS 87 in the Deutsch-Niederländischen Windkanal (DNW) (Germany) wind tunnel to analyze aerodynamic noise emission [4], [5],[7].

More precisely:

- The pantograph was placed on a fixed metal sheet, flushed with the nozzle lower edge, and positioned at 3.43m from the wind tunnel nozzle output section (see figure 1),
- The pantograph was tested in its mean working condition (approximately opened at 1.6m from the train roof),

Experimental tests were conducted at different flow speeds: 32m/s, 48m/s, 64m/s, 78m/s,

A B&K microphones array (vertical antenna) was placed at a distance of 4.89m from the pantograph symmetry plane.

Fig.9 shows a sketch of the experimental test apparatus. Maximum wind speed was about 78m/s with a turbulence intensity being less than 0.2%.

As a result of the experimental tests in all above mentioned flow conditions, the time-domain signal of each microphone was acquired. The SPL in frequency domain with a frequency resolution of 11.6Hz, was then acquired.

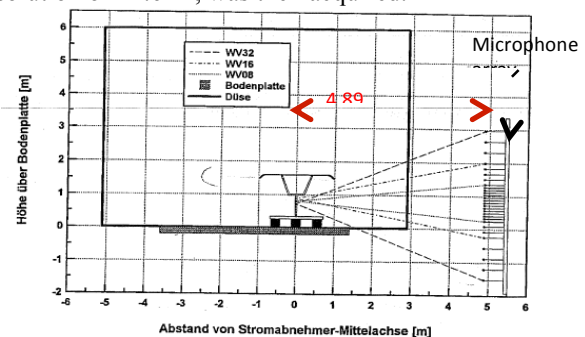


Fig. 9: experimental wind tunnel test apparatus

A summary of the measured results, is reported in next Figure 11, where the experimental overall SPL at different operating speed conditions are shown.

It has to be noted that the curves show similar trends, even if overall translated with reference to the flow velocity. They present a descendent behavior of about 10 dB in the 100-1000 Hz frequency range. A more noise abatement of about 20 dB is present in the 1-5 kHz frequency range. A noise peak at approximately 250Hz is more evident in the 78 m/s speed condition.

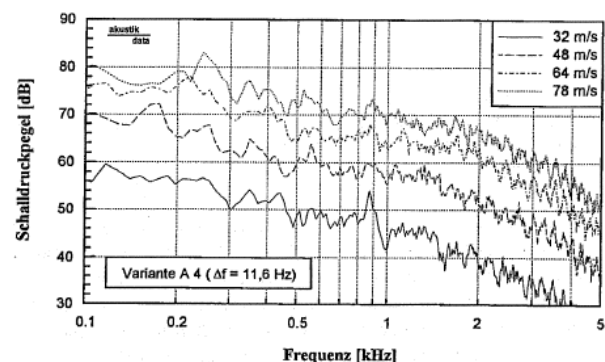


Fig. 10: experimental pantograph aerodynamic noise SPL (dB)

In Figure 10, the equivalent SPL expressed in dB(A) between 100Hz and 5 kHz, at different train speeds are reported.

32 m/s [dB(A)]	48 m/s [dB(A)]	64 m/s [dB(A)]	78 m/s [dB(A)]
71,0	82,8	90,9	96,3

Fig. 11 Experimental overall SPL dB(A)

VI. ANALYTICAL FORMULATION

To evaluate analytically the noise produced by pantograph has been used a provisional method developed for the first time by M.G. Smith and L.C. Chow. This method was developed to predict the commercial aviation airplanes landing gear.

The source of noise in the model are cylindrical elements that compose the structure under investigation.

The method is based on experimental data so it can be considered a semi-empirical model. To obtain a general aeroacoustic model applicable in different fields the data have been scaled in dimensionless parameters. The frequency has been transformed in the Struhal number (1).

VII. SPECTRAL FUNCTION

The principle on which the method is based on consist in the use of some semi-empirical constants, used in spectral functions, to simulate the source behavior for a single component.

For the cylinders used to schematize the pantograph the Struhal number, using its diameter as characteristic dimension, is about 0.2.

The spectral function utilized are dependent from Struhal number, different for each cylinder.

The used spectral function can be written as:

$$f(S) = \frac{a_1 S^N}{a_2 + a_3 S^N + a_4 S^{2N}} \quad (2)$$

the a_i coefficients are empirical constants; a_4 and a_2 govern the sound level at high and low frequencies respectively, a_3 the maximum value, changing a_1 the curve move up and down, N is directly proportional to curve growth rate. These parameters are dependent from the specific problem and they must be founded by experimental tests.

VIII. DIRECTIVITY

The directivity effects are kept into account using a specific corrective coefficient (DF). They are due to the different

orientation of cylinder axe with respect to the receiver. For a single cylinder in a free flux the DF coefficient can be expressed as

$$D_F = 1 - 0.66 \cos^2 \varphi \quad (3)$$

where φ is the angle between velocity direction and the receiver. The value 0.66 is an empirical constant that reduce the value of DF.

IX. PANTOGRAPH DISCRETIZATION

The pantograph has been divided in four principal components:

- Arm
- Trapezium and diagonal beam
- Arc

For every component a more fine discretization is done. The main components have been simulated like cylindrical elements the small elements have been neglected.

X. MODEL EQUATION

For cylindrical components the expression for quadratic pressure in free field for Smith and Chow model is

$$p^2 = (\rho c^2)^2 D_F \frac{M^6}{4\pi R^2} l d \frac{a_1 S_t^N}{a_2 + a_3 S_t^N + a_4 S_t^{2N}} \quad (4)$$

a first modification has been introduced to keep in account the relative orientation between the axe of cylindrical components and the velocity direction.

$$p^2 = (\rho c^2)^2 D_F \frac{M^6}{4\pi R^2} l \sin(\varphi) d \frac{a_1 \sin^2(\varphi) S_t^N}{a_2 \sin(\varphi) + a_3 S_t^N + a_4 S_t^{2N}} \quad (5)$$

where φ is the angle between cylinder axe and train speed.

In equations (4) and (5) c is the speed of sound (m/s), M the Mach number, ρ air density (kg/m³), D_F the directivity factor showed in 4.3, l and d length and diameter of cylinder respectively, R the receiver distance.

XI. HIGH FREQUENCY CORRECTION

Equations (4) and (5) are developed in the smooth surface condition. The real case is so far from this as the presence of gaps, bolts, notches is very consistent along the elements. These elements are very small and can stop the vortex diffusion process generating high frequency noise but they are not relevant at low frequencies.

The total noise produced by a single element is considered the sum of two functions. The first is the noise of the element calculated according to (5). The second is a function having the same form of (4) but different coefficients in which the Struhal number is calculated with a characteristic length of

millimeters applying a high frequency correction to the spectrum.

The final relation of Smith and Chow can be written as:

$$p^2 = \alpha p_f^2 + \beta p_d^2 \quad (6)$$

in which p_f is the contribute of the elements, p_d the high frequency correction. The coefficients α and β are experimental constants.

XII. TOTAL NOISE CALCULATION

The global noise spectrum is next calculated adding the single element noise spectrum.

The level is expressed in dB scaling by the reference pressure $p_{ref} = 20 \mu\text{Pa}$.

$$SPL = 10 \text{Log}_{10} \left[D_W \left(\sum_s \frac{p_s^2}{p_{ref}^2} \right) \right] \quad (7)$$

XIII. PRELIMINARY TEST FOR FORMULA'S VERIFICATION

Some measures have been done in wind tunnel to validate the Smith and Chow model and to find the right set of constant for spectral function. In particular three different diameters have been tested (8 mm, 12 mm and 40 mm) with a flux velocity of 40 m/s.

In this case the Strouhal number is about 0.2 and Reynolds in the magnitude of 104. The acquisition time was settled at 5 seconds.

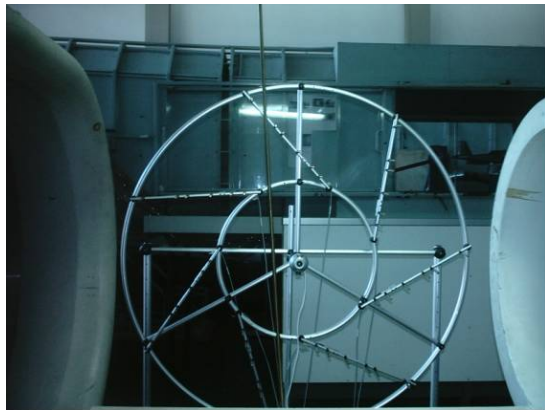


Fig. 12: experimental antenna set up

XIV. MEASURE ON SINGLE CYLINDER ELEMENT

For each cylinder three different inclination (0° , 15° , 35°) have been tested.

In Figure 13 the results for 8 mm diameter cylinder and 0° inclination are shown.

In Figure 14 a curve comparison is showed for the 8 mm cylinder at different inclinations.

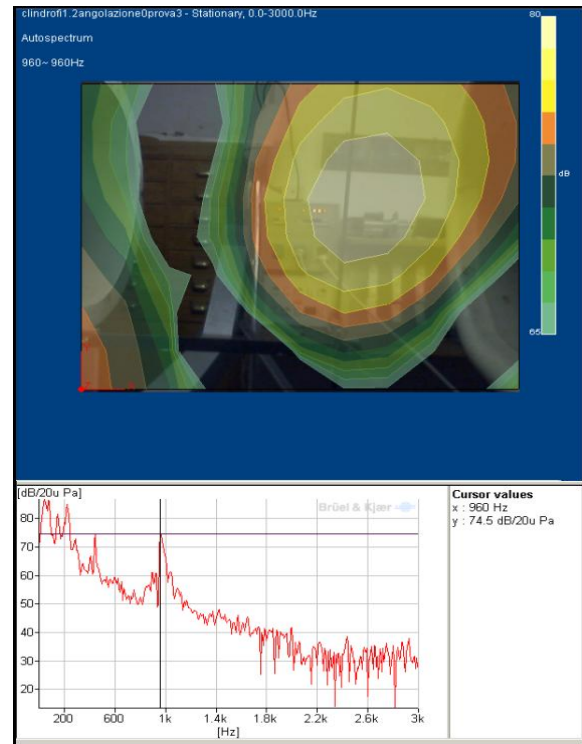


Fig. 13: 8 mm diameter and 0° inclination cylinder experimental noise

From Figure 14 is, also, evident that the noise produced by the cylinder decrease with the decreasing of angle between cylinder and his axes. The experimental results seem to be coherent with the correction of equation (5).

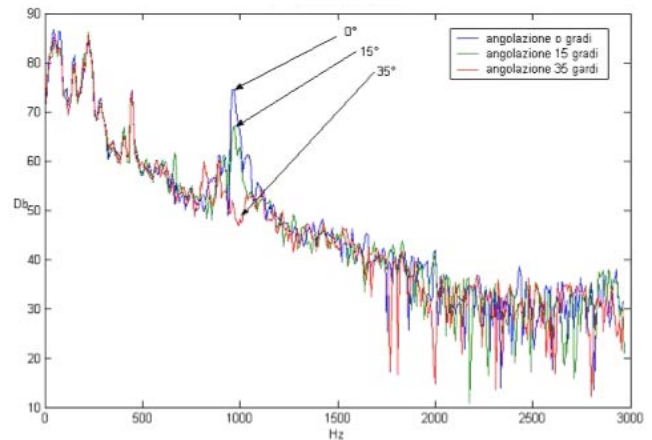


Fig. 14: 8 mm cylinder, different inclinations comparison

XV. THE SSS87 AEROACOUSTIC MODEL

The MATLAB® routine implemented to predict the pantograph's noise emission will be explained in this paragraph.

An M-File with 3 sub-functions has been developed. Basically, the main function workflow can be synthesized as follows:

- The first few rows of the routine let the user select the pantograph that has to be analyzed (at this time just one pantographs have been analyzed (the SSS87), the desired train speed and the distance where the noise has to be computed (it has been set to 4.89m, for comparing analytical results with experimental ones).
- In order to use the Smith & Chow formula, the pantograph has to be simplified into simpler elements. Each pantograph element is considered as a cylindrical rod. The M-File loads the elements dimensions from a properly formatted text file: it is composed by 4 columns (element length, diameter, inclination angle against speed vector and number of elements with the same characteristics) and “n” rows where “n” is the number of different elements in the pantograph.
- The frequency vector is generated. For the purpose of this activity, a frequency step of 8Hz has been used, with a minimum frequency of 100Hz and a maximum of 5000Hz.
- Using a sub-function, the mean square far field pressure for each element at the observer radius R is computed, using the mentioned Smith & Chow modified formula (5) and (6).
- Single elements pressure spectra are transformed into Sound Pressure Level spectra through the formula (7).
- Now the single elements pressure contributes are linearly summed and the SPL spectrum of the entire pantograph is computed.
- Also the arm, the trapezium and the arc contributes are computed summing the relatives cylindrical rods.
- The SPL spectrum of each element is filtered with the A-weighting procedure using the A-curve (Fig. 15). The spectrum after the filter application is shown in Figure 16.
- The overall SPL(dB(A)) is calculated for the entire pantograph and its main parts (arm, trapezium and arc).
- Lastly, the M-File loads the experimental results (Sound Pressure Level spectrum at different train speed measured at a distance of 4.89m from the pantograph symmetry plane) and compares them with the analytical ones calculated in terms of sound spectra and SPL overall level A-weighted (in order to compare data, the imported SPL(f) data are interpolated into a common frequency vector).

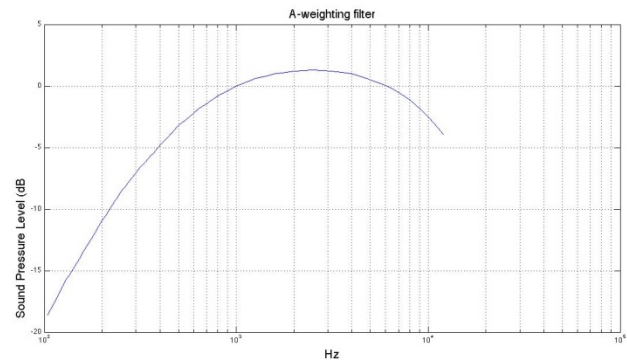


Fig. 15: A-weighting curve

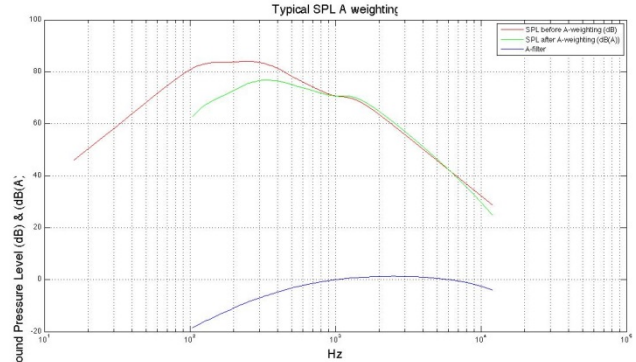


Fig. 16: Example of SPL curve after the A-weighting application

XVI. SSS87 PANTOGRAPH'S SIMULATION

The previously explained MATLAB® routine has been used to predict SSS87 pantograph's acoustic emission: as experimental data about this pantograph acoustic emission were available, it has been possible to compare analytical results with the experimental ones and validate the MATLAB® routine.

Since for this pantograph there weren't any 3D CAD models, the pantograph has been reconstructed using some 2D CAD where its main dimensions were clear (Figure 17).

The pantograph is simplified by a sum of cylindrical rods, each one characterized by diameter, length and inclination against the speed vector. Table 1 shows the schematization of the SSS87 pantograph: 17 different kinds of elements were identified, some of them repeated 2 or 4 times as stated in the last column of the Table. Moreover, this table is loaded into the M-File as explained in the previous chapter at the point two.

Component's name	Length (mm)	Diameter (mm)	Φ (degree)	Number of elements
Arm inferior cylinder	601,74	79,95	0,000	1
Arm riser cylinder	1593,48	83,68	156,000	1
Arm tie rod	1000,00	34,16	149,000	1
Arm superior cylinder	268,78	78,00	0,000	1
Trapezium inferior cylinder	284,21	59,48	0,000	1
Lateral cylinder	1729,97	29,39	17,300	1
Trapezium first cylinder	1247,19	61,10	17,054	2
Trapezium second cylinder	844,84	45,83	17,054	2

Trapezium tie rod	1326,08	8,34	17,054	2
Mean trapezium cylinder	264,71	36,08	0,000	1
Trapezium superior cylinder	1115,56	35,10	0,000	1
Lateral cylinder	518,86	39,81	0,000	2
Arc superior rod	1002,27	41,83	0,000	2
Arc first horn	146,41	27,27	0,000	4
Arc second horn	144,96	15,88	0,000	4
Element 1	281,45	27,80	0,000	2
Element 2	67,25	27,80	0,000	2

Table 1 – SSS87 pantograph’s elements schematization

The frequency step used in the simulation is 8Hz (for being as close as possible to the experimental simulation).

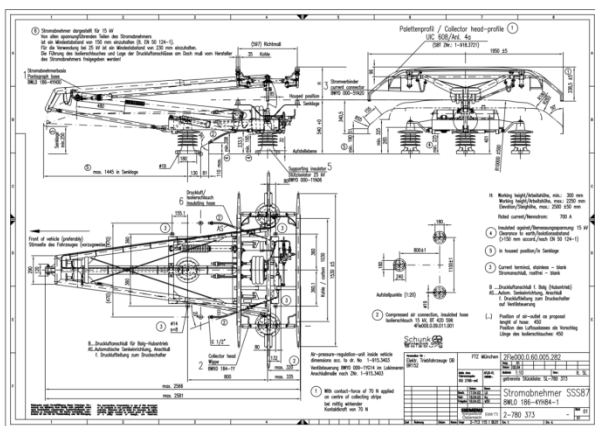


Figure 17 – SSS87 pantograph’s structure

The Φ angles reported in Table are relative to the pantograph in its mean operating configuration, where the top part of the arc is at 1.6m of height from the train top surface.

The pantograph has been analyzed at different train speeds: 48 m/s, 64 m/s, 78 m/s (as reported in the experimental data).

XVII. SSS87 RESULTS

The MATLAB® routine has been run several times, each time changing the shape function coefficients, in order to smooth the spectra to best fit the experimental trend.

It is important to underline that aeroacoustic noise is generally derived from the sum of the “tone shaped” contribution (due to the rod elements vortex shedding induced noise) and the aerodynamic “flow noise”. Inside the described formulation, these contribution have been merged by the use of smooth tone-like contribution shape. As a general rule, the shape has been adjusted to avoid “zero noise” frequency ranges. Obviously this adjustment have to be decided on the basis of single elements dimension (that define the spectral frequency center). This choice will probably reduce the accuracy in the determination of the peak noise, but would not

much effect the overall noise determination.

Within the present work, once reached the desired precision level, the shape function coefficients have been fixed. The results for the SSS87 pantograph are shown in the next pages.

In the next table the comparison between experimental overall sound levels (A-weighted) and analytical ones is shown.

Speed (m/s)	Experimental overall value dB(A)	Analytical overall value dB(A)
48	82,8	79
64	90,9	89,4
78	96,3	96,4

Table 1 – SSS87 pantograph: Comparison between analytical and experimental results

As it can be deduced from the table above, the analytical overall level grows with a speed law very close to the experimental one (Fig. 8).



Fig. 18: Experimental and Analytical Overall SPL(dB(A)) function of train speed

The following pictures report the analytical results (pink curves) compared to the experimental ones (green curves).

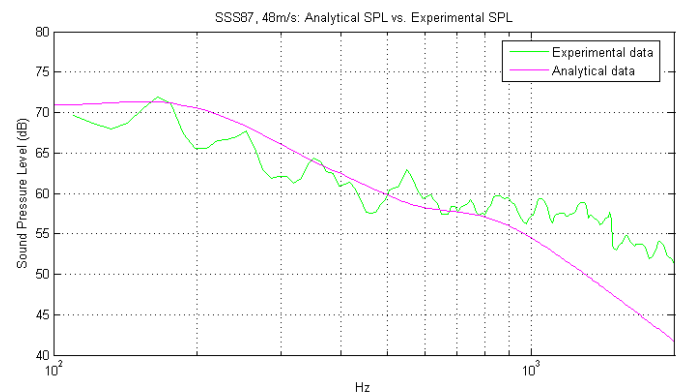


Figure 19: SSS87 analytical vs. experimental result at 48m/s



Figure 20: SSS87 analytical vs. experimental result at 64m/s

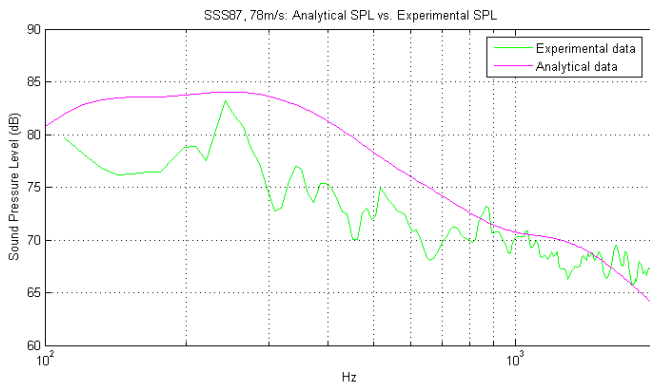


Figure 21: SSS87 analytical vs. experimental result at 78m/s

The SPL curve presents a peak at 180Hz at a train speed of 48 m/s that moves to 280Hz when the train reaches the speed of 78 m/s; the peak increases its amplitude of almost 13dB (from 71dB to 84dB) with a train speed increasing of 30 m/s (going from 48 m/s to 78 m/s).

In all the train speed configurations, the SPL curve loses approximately 15dB when it reaches the 1000Hz and then it decreases of other 15dB for the next 1000Hz.

It is clear that, with an analytical formulation, all the “mini-peaks” resulting from the experimental tests cannot be reproduced. Nevertheless, this formulation returns important information about the behavior of the SPL curve and about its overall value.

For this reason it is preferable to look at the results with an octave band spectrum (it gives back information about the sound energy more than the SPL peaks).

In the next pictures the octave band sound spectrum for each speed is illustrated.

With the octave spectra it is clear that the major sound energy contribute is given back under 1kHz, in fact in the overall level calculation, the SPL peak and the values around it are the ones that “weight” more.

As a result, it can be inferred that the more the train speed reaches values similar to the A320 landing speed (around 260 km/h \approx 72 m/s) the more the implemented Smith & Chow formula increases its precision, this is due to the fact that this formula has been implemented for predicting the aerodynamic noise emitted by the A320 landing gear, so its accuracy is higher in the speed range near the A320 landing ones.

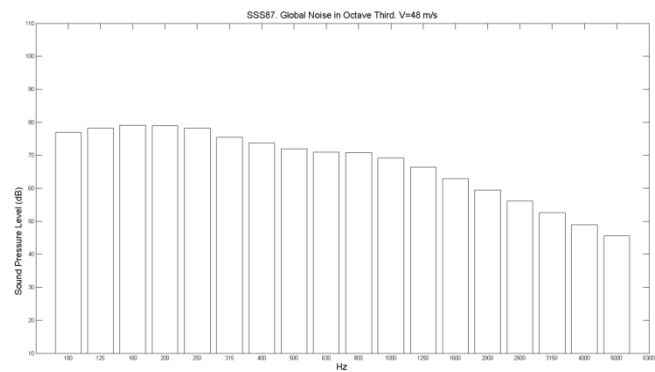


Fig. 22: SSS87 octave band sound pressure spectrum at 48m/s

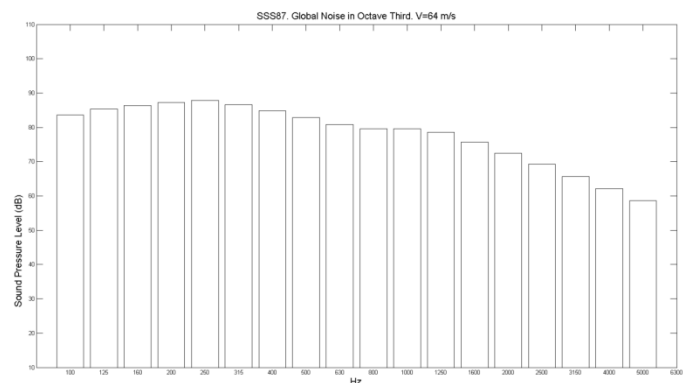


Fig. 23: SSS87 octave band sound pressure spectrum at 64m/s

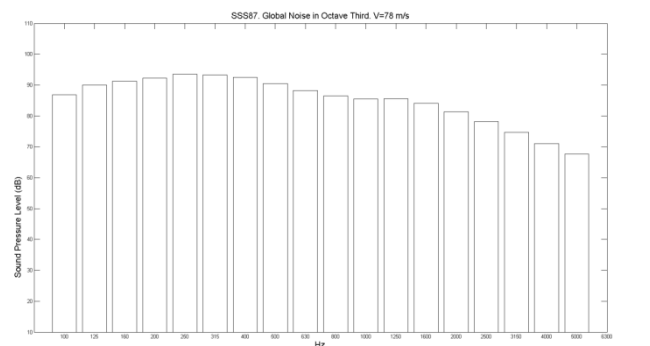


Fig. 24: SSS87 octave band sound pressure spectrum at 78m/s

XVIII. CAA ANALYSIS

In order to numerically compute the acoustic emission of the pantograph SSS 87, several steps have been executed for building up and then analyze the numerical model: starting from a 2D drafting, a 3D CAD model of the fluid control volume around the structure has been created and then meshed and analyzed according to defined boundary conditions.

Because of experimental results demonstrated a similar trend of the SPL curves at different train speeds, the CAA analysis of the pantograph have been run in the highest speed condition (78m/s), corresponding to the noisiest operating condition, also to reduce the calculations time.

XIX. GEOMETRICAL DESIGN

In this paragraph, a description of the design procedure is reported.

Because there was only a 2D pantograph design model, a 3D CAD model of the pantograph SSS 87 has been built using the software CATIA V5® (Figure 25). Considering the purpose of the model, it has been built up very carefully:

- In order to simplify the meshing operation and the computer solving time, small features of the pantograph, such as screws, cables or holes, have been neglected.
- Considering the maximum frequency measured during the experimental analysis (5 kHz), small components of the structure has been neglected

The pantograph in the 2D drafting is in its “sleeping” condition; in order to compare the numerical simulation with the experimental ones, it has been necessary to develop the 3D model in its mean working condition.

Once the 3D pantograph CAD model has been designed, the surrounding fluid control volume has been created.

Specifically, a cylindrical control volume, length of 3.8m and a diameter of 3m, is realized.

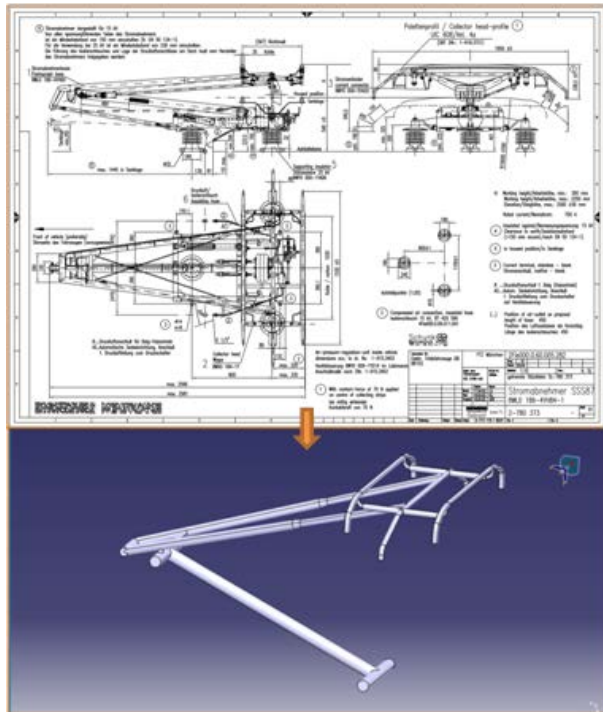


Fig. 25: 3D CAD model obtained after 2D manipulation

In order to simplify the model and reduce the computing time a symmetry plane of the pantograph was considered.

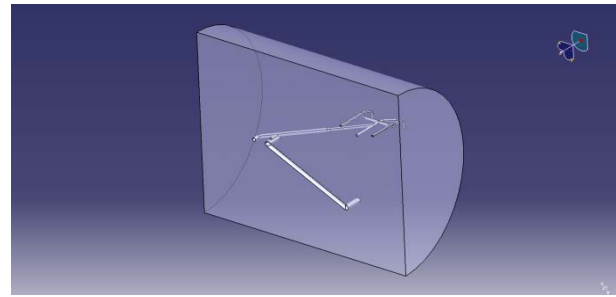


Fig. 26: Fluid control volume around the object

The mesh process represents an important operation to achieve with good accuracy numerical results. For this reason, the mesh has been realized finer close to the wall boundaries and around the object to study, in order to take into account the viscous effects inside the boundary layer. Far away from the body the flow is undisturbed, so the mesh can be coarser. According to the acoustic analysis, the mesh has to be fine enough in the entire fluid volume in order to allow the sound wave propagation. The maximum element dimension has to be considered not greater than 1/5 of the considered wavelength.

Figures 27 and 28 show the entire volume and a zoom of the realized mesh model, respectively.

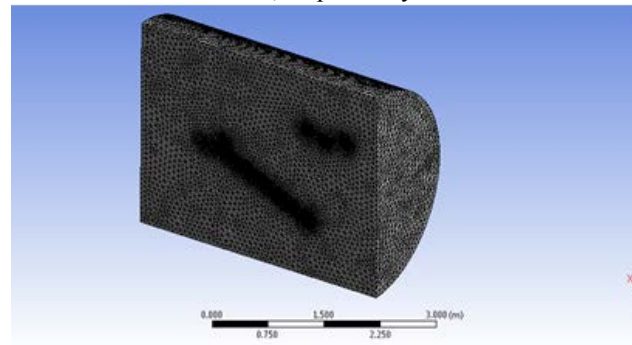


Fig. 27: control volume mesh

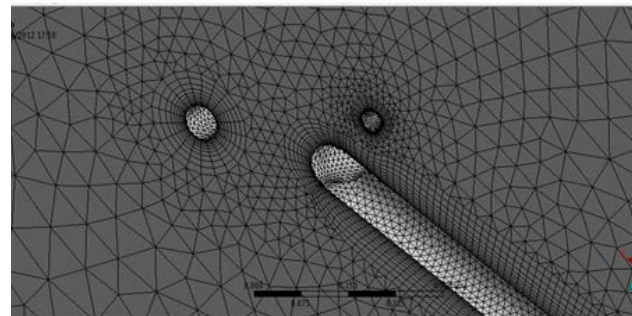


Fig. 28: detailed control volume mesh

For the purpose of the analysis tetrahedrons elements have been chosen. The maximum length of element's edge is approximately 0.04m (according to the acoustic analysis requirements). Because of, the pantograph surfaces represent wall boundaries, the mesh has been thickened in their proximities, using a transition ratio during the inflation process of 0.5 (it means that in the proximity of a wall, the elements will halve their dimensions).

XX. ANALYSIS CONDITIONS

FLUENT® solver with the k- ϵ realizable simulation model, characterizing non-stationary phenomena such as vortex shedding, three-dimensional flow field was used for calculations [3]. Table 3 shows the applied characteristics for computational domain.

The no-slip condition for velocity is applied to the model surface. The outlet is set to an outflow boundary condition, which dictates a zero diffusion flux.

Specifically:

- A transient analysis is realized in order to take into account vortex shedding phenomena,
- The used turbulence model is the k- ϵ realizable;
- Both the “Time step” and “Number of time steps” parameters have been set according to acoustics requirements; in fact, the time step determines the highest frequency that can be measured on the basis of the Nyquist-Shannon sampling theorem, [5], and the the frequency resolution of the signal.

Type of analysis	Transient, pressure-based
Fluid dynamic model	k- ϵ realizable
Wall conditions	Standard wall function
Inlet boundary condition	Uniform velocity (78 m/s)
Outlet boundary condition	Uniform pressure
External surface condition	Wall with 0m RH
Object surface condition	Wall with 1e-3m RH
Residual values	1e-5
Aero Acoustics model	Ffwoacs Williams - Hawkings
Sound source	Body surface
Number of receivers	35
Time step	2,5e-4 s
Number of time steps	400
Max iteration per time step	300

Table 3: CAA Analysis settings

Figure 29 reports the simulated microphone array replying perfectly the experimental position. The array was composed of 35 microphone receivers at a distance of 0.4 m from each other (width 2.4 m and height 1.6 m).

In order to simulate the acoustic far field condition, the microphones array has been set at a distance 1m from the pantograph's symmetry plane.

A set of computational tests have been performed in order to verify the robustness and reliability of the model:

- Robustness check: three different mesh model have been realized in order to verify the goodness of the results.
- Speed Sensitivity check: the aim of the test is to verify that the model was stable. Three different speeds have been chosen: 77m/s, 78m/s and 79m/s. The results have proven that the output of the system does not change significantly.

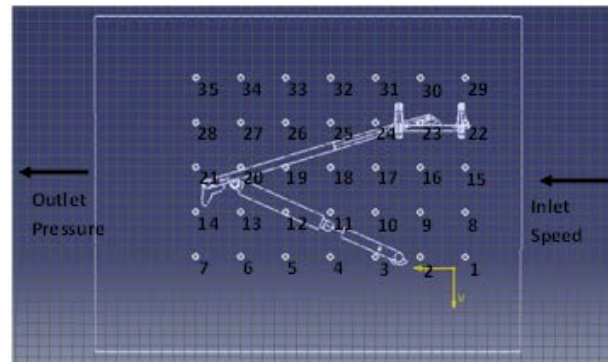


Fig. 29: numerical receivers array

XXI. CAA RESULTS

In Figure 30, the instantaneous fluid flow around the pantograph is shown; the flow field has a highly 3D behavior, starting from a uniform condition of 78m/s (applied normal to the inlet surface), the fluid shows an acceleration in proximity of the object and some turbulent wakes behind it are present. In fact, the fluid separates on the sides of the object and the streamlines cannot follow its profile until the end of it, generating low pressure and turbulent regions.

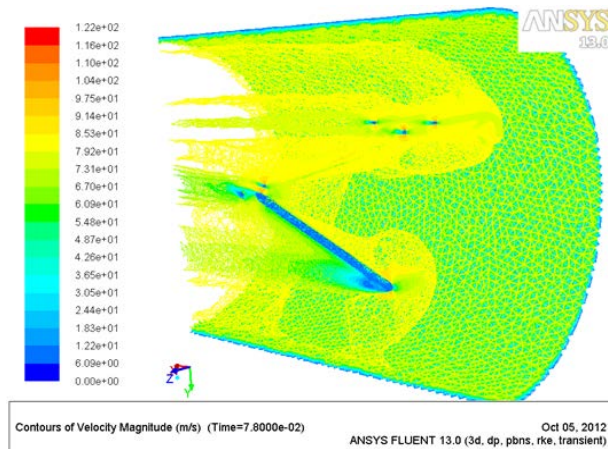


Fig. 30: instantaneous numerical contours of velocity around the pantograph

Looking at the evolution of the flow through time, it is interesting to notice that despite the uniform and stationary inlet condition, the flow field inside the control volume evolves through time: this is due to the fact that turbulent flows are highly non stationary phenomena.

Unfortunately, due to the turbulent model used, after a first non-stationary time interval, the flow tends to become stationary: looking at the evolution of the acoustic pressure during the acquisition time at a fixed receiver (Figure 31), it is evident that after a first period of transient signal, the pressure becomes stationary for approximately 0.05s (half of the sampling time); this means that after 0.05s, the flow in the control volume becomes stationary.

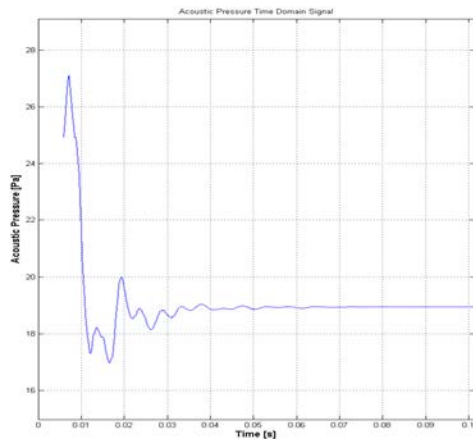


Fig. 31: acoustic Pressure vs. Time at receiver

Analyzing a signal composed of a non-stationary part and a stationary one, will give back wrong results. The reason is that an acoustic occurrence has to be measured with a microphone, but analyzing a signal as the one in Fig. 10 is like measuring the desired acoustic occurrence and continuing the measure even after the phenomenon ends. This procedure is obviously wrong and so, in order to have realistic results, is correct to analyze only the non-stationary part of the signal (the actual acoustic phenomenon). In order to realize this, the “Pressure VS Time” signal has been trimmed at 0.05s, so that the acoustic post-processing is computed only on the non-stationary part of the phenomenon.

As done in the experimental post-processing, the pressure at the receivers have been averaged.

In Figure 32, the numerical and experimental mean SPL emitted by the pantograph between 100Hz and 2000Hz are shown. The frequency behavior of the numerical model strictly follow the experimental one; the numerical simulation has been able to reproduce almost every single noise peak detected in the experimentation with just a slight frequency gap between experimental and numerical peaks due to the different frequency resolution used.

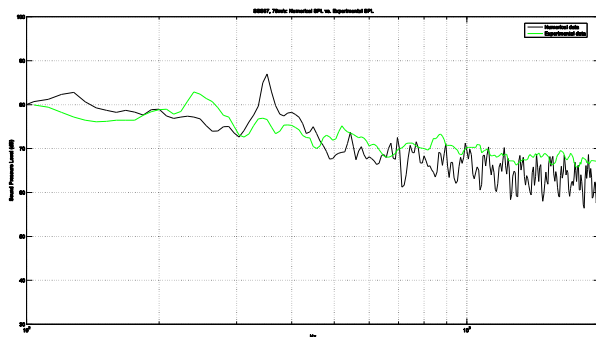


Fig. 32: numerical and Experimental SPL frequency spectrum at 78m/s

In table 4, the SPL Overall value at different train speed is shown; in order to read the values in the table, it is important to do the following assumptions:

- The numerical simulation has been performed at flow speed of 78m/s, while the numerical values at

64m/s and 48m/s are the results of an analytical manipulation of the SPL, considering the SPL variation with speed given by the experimental results.

- The numerical simulation has been capable of generating an SPL up to 2kHz, while the experimental analysis has gone up to 5kHz; the experimental SPL Overall values have been calculated between 100Hz and 5kHz, while the numerical SPL Overall values have been calculated between 100Hz and 2kHz; that is the reason why the numerical and experimental SPL Overall values presents some differences.

SPL Overall Value dB(A)					
Experimental			Numerical		
48m/s	64m/s	78m/s	48m/s	64m/s	78m/s
82.80	90.90	96.30	79.94	86.11	92.32

Table 4: comparison between experimental and numerical Overall SPL at different speeds

Moreover, by the use of the numerical simulation, the regions of the object causing more noise have been detected. It has been, in fact, discovered that the regions that generate more noise are the central part of the arc and the junction between the trapezium and the arm (the knee, evidenced in Figure 33), these are the same results found during the SSS 87 experimental simulations.

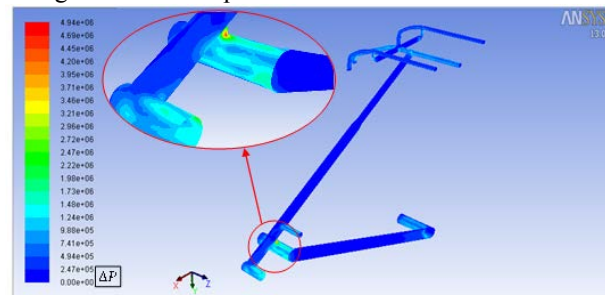


Fig. 33: numerical noise emission power contour map on the pantograph

XXII. OVERALL RESULTS DISCUSSION

Next reported Table 5, show a synthesis of the results referred to the identified speed conditions, as derived from the analytical, numerical and experimental models.

SPL Overall Value dB(A)								
Experimental			Analytical			Numerical		
48 m/s	64 m/s	78 m/s	48 m/s	64 m/s	78 m/s	48 m/s	64 m/s	78 m/s
82.8	90.9	96.3	78.5	88.9	96.0	79.95	86.1	92.3

Table 2 – SSS87: Overall SPL values (dB(A)) comparison after the signal post-processing

As a general rule, the numerical simulation underestimates the SPL overall noise from 2.8dB(A) to 4dB(A), this is a

good results considering the fact that the experimental tests have been carried out with a noise frequency analysis between 100Hz and 5000Hz, while the numerical simulation runs “just” up to 2000Hz. At all train speeds a noise contribution over 2000Hz is always present (even if from 2kHz to 5kHz, the SPL loses 20dB), so it can be supposed that in the numerical simulation one or two decibels are lost in that frequency range.

In the next images, the SPL(dB) frequency spectrum of the numerical, experimental and analytical data at different train speeds.

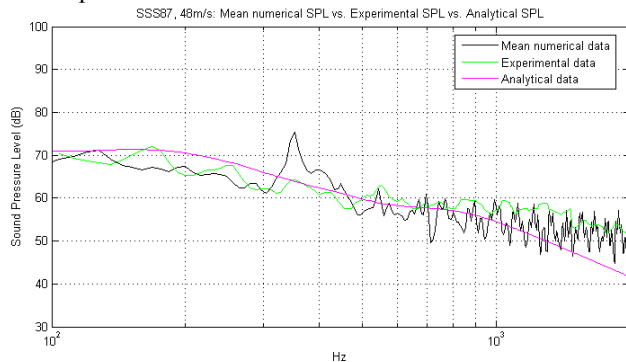


Fig. 34: Mean numerical SPL results vs. Experimental and Analytical results at 48m/s (4.89m distance) after the signal post-processing

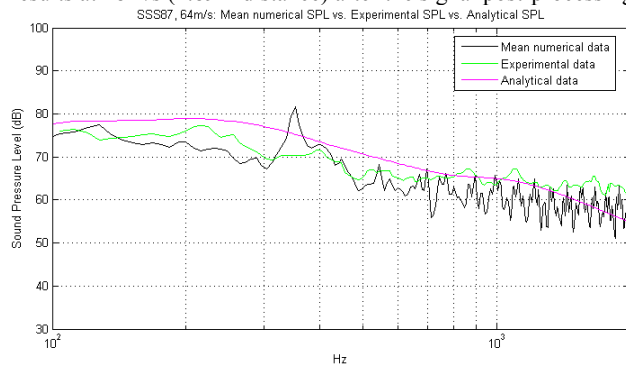


Fig. 35: Mean numerical SPL results vs. Experimental and Analytical results at 64m/s (4.89m distance) after the signal post-processing

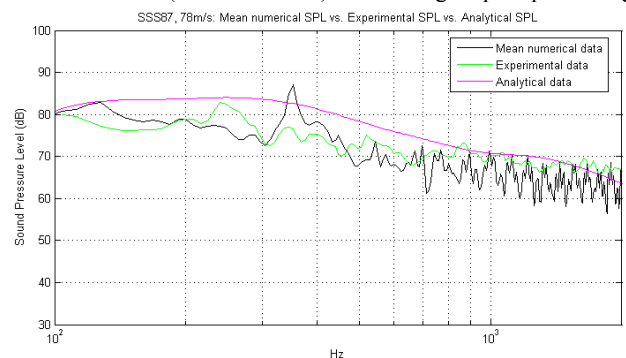


Fig. 36: Mean numerical SPL results vs. Experimental and Analytical results at 78m/s (4.89m distance) after the signal post-processing

The frequency behaviors of the numerical model noise strictly follow the experimental ones. The numerical simulation has been capable of reproducing almost every single noise peak detected in the experimentation with just a slight frequency gap between experimental and numerical peaks due to the different frequency resolution used. In the

previous images one of the advantage of elaborating a numerical model is shown: the analytical formulation follows the general behavior of the noise curve, but it is not able to reproduce a frequency local characterization, while the numerical simulation it may be slightly underestimates the noise produced by the pantograph, but is able to reproduce its frequency behavior in detail.

The amplitude gap between the experimental results and the numerical ones has to be assigned to different reasons:

Geometry simplification: in order to properly mesh the control volume, the geometry of the pantograph has been simplified, deleting all the holes, screws, cables and fillets that make the geometry too complex to be analyzed.

Fluid-Structure interaction neglected: the object has been considered as a infinite rigid wall, that does not interact with the fluid.

Fluid-dynamic model simplified: in order to look at Von Karman vortex shedding in the object's wake, a Large Eddy Simulation analysis with a bigger control volume and a finer mesh should have been used. For processor capabilities and time requirements it has been impossible to do it, but a simplified model has been used: a k-eps realizable model that gives back a slight oscillation of velocity, turbulence and pressure around the object and in its wake.

XXIII. CONCLUSIONS

As a general conclusion of the activity, it can be stated that numerical model for the prediction of high-speed train pantograph's aerodynamic noise has been developed.

The numerical model strictly reproduces the real sound pressure level spectrum emitted by the pantograph.

Through the use of the numerical model it is possible to detect the part of the pantograph generating more noise.

For these reasons it can be said that the aerodynamic noise prediction method developed is efficient, reliable and accurate. The method will so used for the prediction of aerodynamic noise emission for a similar high speed train pantograph system.

The analytical model has the same precision of numerical model for speed of 48 m/s but is more precisely at higher speed. The error goes zero for very high velocity. The reason of these behavior of the model is the model is developed for landing gear of commercial aviation and is full precise at typical landing velocity.

It can be conclude that both models are very accurate and can be used for a preliminary evaluation the analytical model and for a finer calculation the numerical one.

REFERENCES

- [1] Smith M.G., Chow L.C., Prediction Method for Aerodynamic Noise from Aircraft Landing Gears, AIAA 98-2228
- [2] Lighthill M.J.: On sound generated aerodynamically. I. General theory, Proceedings of the Royal Society of London. Series A, Mathematical and Physical Sciences 211(1107), 564–587 (1952)

- [3] Ffowcs Williams J. E., Hawkings D. L., Sound generated by turbulence and surfaces in arbitrary motion, London: Philosophical Transactions of the Royal Society of London, (1969)
- [4] Ingenieurbüro akustik-data, Dipl.-Ing. B. Barsikow, Bestimmung der Schallemission verschiedener Varianten des Stromabnehmers SSS 87 im Deutsch-Niederländischen Windkanal (DNW), Bericht Nr. 97/2, Kirchblick 9 D-14129 Berlin, (1997)
- [5] Viscardi M., Rusciano N., Iadevaia M. & Siano D., An optimization process experience for HVAC noise emission and flows distribution inside a passenger's train wagon, 16th International Congress on Sound and Vibration 2009, ICSV 2009, pp. 3334.(2009)
- [6] Shannon C. E., Communication in the presence of noise, Proc. Institute of Radio Engineers, vol. 37, no. 1, (1949)
- [7] M. Viscardi, D. Siano, P. Napolitano, F. Donisi, An analytical model for the aerodynamic noise prediction of an high-speed train pantograph, Latest Trends in Circuits, Systems, Signal Processing and Automatic Control, ISSN: 1790-5117, ISBN: 978-960-474-374-2, 2014.

M. Viscardi was born in 28/01/1970 in Naples, he graduated at University in Naples in Aeronautical Engineering on 1994. PHD in Aerospace Engineering in 1998. From November 2006 Assistant Professor of Structural Testing at the University of Naples "Federico II".

Its main field of interest are structural dynamics, acoustic and Vibration, Active noise and vibration control, advanced NDT technologies, as well the piezoceramic based sensors and actuators technologies and the electronic devices for acquisition, control and communication. For what concern this latter aspect, two new products have been designed and market placed within the last ten years. From April 2002 to the end 2006 Member of the Scientific Committee on Ministry of Industry for the Research and Development programs.

Member of Editorial board of several scientific journal, has been scientific coordinator of more than 15 research and Innovation projects for PMI. Author of more than 50 scientific works and more than 70 thesis degree. He held more than 30 training courses in the reference research field at post graduate and master level.

Daniela Siano was born in Naples in 06/01/1969 Italy, and graduated in Aeronautical Engineering at the University of Naples "Federico II", Italy in 1994.

She is currently a Researcher at the National Research Council of Italy (CNR) in the field of Acoustic and Vibration. She is responsible of Acoustic and Vibration Laboratory in her Institution. Expert evaluator within the EU 6th and 7th Framework Research Programme, Transport-Aeronautics in 2006 and 2007.

Referee for International Journals and she is author of about 70 Scientific Papers published on International Journals and Conferences Proceedings and tutor of more than 40 thesis degree.